LAWRENCE
LIVERMORE
NATIONAL
LABORATORY

UCRL-JRNL-231451

Ab initio studies of niobium defects in uranium

S. Xiang, H. Huang, L. Hsiung

June 4, 2007

Journal of Nuclear Materials

Updated October 14, 2003

Ab initio studies of niobium defects in uranium

Shikai Xiang and Hanchen Huang [1]
Department of Mechanical, Aerospace and Nuclear Engineering, Rensselaer Polytechnic Institute, Troy, New York 12180

L. M. Hsiung
Lawrence Livermore National Laboratory, Chemistry, Materials, and Life Sciences Directorate, P.O. Box 808, L-352, Livermore, CA 94551, USA

Uranium (U), with the addition of small amount of niobium (Nb), is stainless. The Nb is fully miscible with the high temperature phase of U and tends to segregate upon cooling below 647°C. The starting point of segregation is the configuration of Nb substitutional or interstitial defects. Using density-functional-theory based *ab initio* calculations, the authors find that the formation energy of a single vacancy is 1.08 eV, that of Nb substitution is 0.59 eV, that of Nb interstitial at octahedral site is 1.58 eV, and that of Nb interstitial at tetrahedral site is 2.35 eV; all with reference to a reservoir of γ phase U and pure Nb. The formation energy of Nb defects correlates with the local perturbation of electron distribution; higher formation energy to larger perturbation. Based on this study, Nb atoms thermodynamically prefer to occupy substitutional sites in γ phase U, and they prefer to be in individual substitutional defects than clusters.

61.72.Ji, 66.30.Jt

I. INTRODUCTION

[1] Author to whom correspondence should be addressed; electronic mail: hanchen@rpi.edu

Uranium (U) has three solid phases: α, β and γ phases.[1,2] Since U is relatively less commonly investigated among solid state physicists, we first briefly describe the atomic arrangements in these three phases; as shown in Fig. 1. The α phase has an orthorhombic structure, and its conventional unit cell contains four atoms, as in face-centered-cubic (FCC) crystals [Fig. 1(a)]. However, the atoms at sites J and K are not at face centers although they are on front and back faces. Further, there are no atoms on the left and right faces, and instead one effective atom L is inside the unit cell.[3] The crystal structure of β [Fig. 1(b)] and [Fig. 1(c)] γ phases are body-centered-tetragonal (BCT) and body-centered-cubic (BCC), respectively. Under ambient pressure, the α, β and γ phases are stable at 0-940 K, 940-1050 K and 1050-1407 K respectively. [1] Because of 5f electrons among other factors, U exhibits abnormal properties such as low temperature charge density waves (CDW) transitions[4,5] and anisotropic thermal expansion.[6]

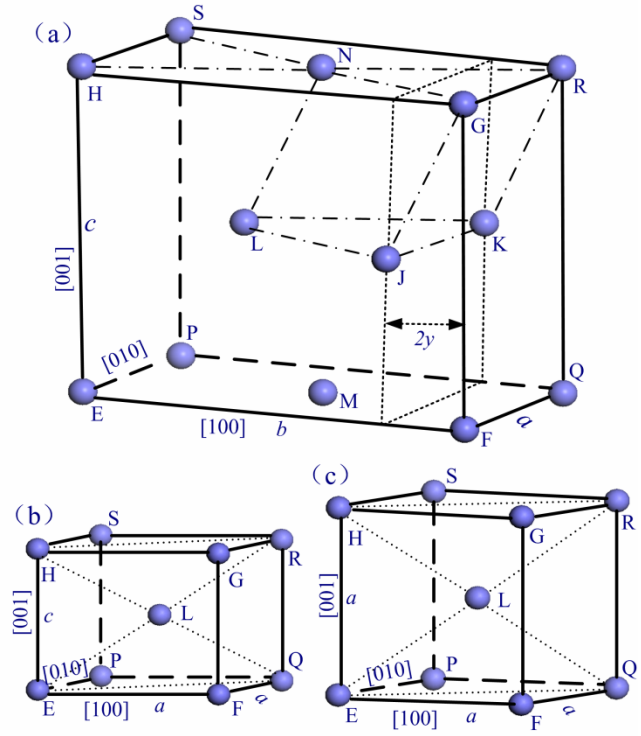

Fig. 1. (Color online) Crystal symmetry of (a) α, (b) β and (c) γ phases, with U atoms shown as spheres and directions shown by Miller indices. The *a*, *b*, *c* and *y* are lattice constants, and atomic labels (such as P and M) are for reference later on.

At least two of the three phases are relevant in making stainless U. In the form of pure solid, U is prone to oxidation. The addition of small amount of Nb significantly improves its corrosion resistance, so as to achieve "stainless" U. Due to the low solubility of Nb in α and β phases of U, Nb is introduced into the high-temperature γ phase of U. Upon quenching, the Nb atoms initially stay at where they were, to improve the corrosion resistance. However, with time these Nb atoms diffuse around and lead to precipitation and formation of new phases at low temperatures. This problem of aging will inevitably affect chemical and mechanical properties of the alloyed U. For example, the precipitation of Nb atoms results in ductility reduction.[7,8] To understand the precipitation processes, it is critical to first examine where Nb atoms sit as they are introduced into the γ phase before quenching.

Atomistic simulations are a convenient tool to study defect configurations. Due to the complex electronic structures of U, classical calculations are generally out of question. Density-functional-theory based *ab initio* calculations offer a unique tool to investigate details of alloy structures. Indeed, such calculations have been applied successfully to studying crystal structure,[9,10] elastic constants,[11] CDW[12] and phase diagram of pure U.[2] Aiming for rigorousness, all these calculations are based on full potentials with generalized gradient approximation (GGA) of the electron exchange-correlation. Once defects are involved, larger simulation cells are necessary to avoid artifacts of simulation cell size dependence. A pseudopotential-based approach has to be used to reduce the computational cost and yet maintain physical rigorousness. This is the case in the studies of point defects in uranium dioxide using norm-conserving pseudopotential methods together with local density approximation (LDA)[13] or with GGA.[14]

This work is also based on pseudopotentials with GGA approximation. Our approach is to test the validity of this method by studying pure U and comparing our results with

literature reports, before using the method to U with Nb defects. The rest of this paper is organized into three sections. In Section II, we present the computational details. In Section III, we first present the results of pure U to demonstrate the validity of the method, and then the results of U-Nb by comparison and contrast with pure U. Finally, in Section IV we summarize the conclusions.

II. COMPUTATIONAL METHOD

Within the framework of density functional theory, we perform all the calculations with plane-wave bases using the projector augmented wave (PAW) method, as implemented in Vienna *ab initio* simulations package (VASP).[15,16] The standard PAW potentials in VASP include $6s^2 6p^6 5f^3 6d^1 7s^2$ valence electrons for U and $4p^6 5s^1 4d^4$ for Nb. As the results indicate later on, inclusion of thee valence electrons is sufficient. We use GGA descriptions for exchange-correlation[17] and set the cutoff energy in plane wave basis expansion as 350 eV both for U and Nb. Except for the test of α phase, our calculations do not include spin-orbital interactions. All the geometric relaxations are performed with a quasi-Newton algorithm using the exact Hellmann-Feynman forces, with a convergence criterion of force being 0.01 eV $Å^{-1}$.

In determining the equilibrium structures of pure U, supercells are the same as primitive unit cells, and k-point meshes are 20 x 20 x 26, 24 x 24 x 22, and 26 x 26 x 26 for α, β and γ phases respectively. These criteria ensure that a convergence of the total energy to be within 1 meV. For α and β phases, which have internal freedom in the primitive unit cells, the starting configuration of the cell shape and internal freedom is based on experimental values. In rigorous calculations, an elastic constant should be the curvature near equilibrium lattice constants.[18] However, in order to compare with existing *ab initio* and experimental data of bulk modulus and its pressure derivative, we here adopt the third-order Birch-Murnaghan equation of state.[19] The two ways of calculations give the same bulk modulus within 1% error. Partial densities of state according to Mulliken population analysis[20] serve to elucidate the importance of f-electrons and to justify the choice of valence electrons.

In determining Nb defect configurations, we use large simulation cells. Three types of defect configurations are: single vacancy, Nb at substitutional site, and Nb at interstitial site. The U here is the BCC γ phase, the supercell size is 3 x 3 x 3 in the unit of lattice constant *a*. The k-point meshes are 6 x 6 x 6, and other parameters are the same as for pure U calculations. These criteria ensure that a convergence of the total energy to be within 10 meV. This value, although larger than the 1 meV for perfect U calculations, is sufficient for defect energy calculations and allows the use of smaller k-point meshes.

The formation energy of a single vacancy is defined as $E_v = E_d - (n\text{-}1)E_U$. Here E_d is the total energy of a simulation cell containing $(n\text{-}1)$ U atoms, and E_U the potential energy of each U atom in a perfect crystal; a perfect crystal without the vacancy would contain *n* U atoms. To minimize system errors, E_U is from the simulation cell containing *n* U atoms. The formation energy of a Nb substitutional defect is defined as $E_s = E_d - (n\text{-}1)E_U - E_{Nb.}$ Here E_d is the total energy of a simulation cell containing $(n\text{-}1)$ U atoms plus an Nb atom occupying a normal lattice site, and E_{Nb} the potential energy of each Nb in a perfect crystal. The formation energy of a Nb interstitial defect is defined as $E_s = E_d - nE_U - E_{Nb.}$ Here E_d is the total energy of a simulation cell containing *n* U atoms plus an extra Nb. In essence, this definition of Nb defect formation energies assumes a reservoir of Nb crystal next to a U crystal.

II. RESULTS

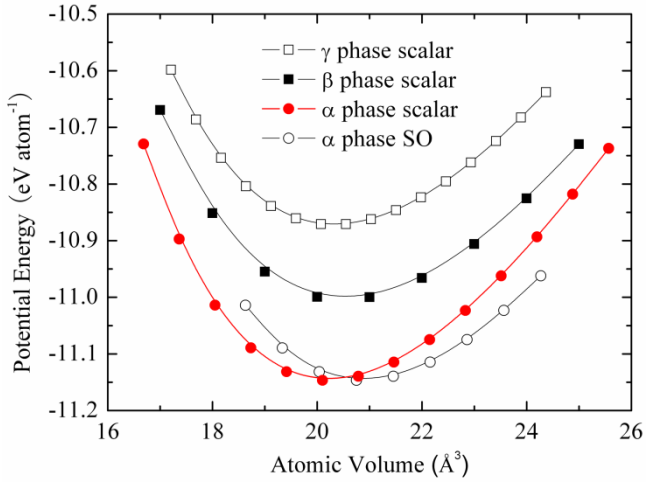

Fig. 2. (color online) Potential energy versus atomic volume for α, β and γ phases of U; with scalar or spinal-orbital (SO) interactions.

In this section, we start from results of pure U, and proceed to those of U-Nb by using the former for comparison and contrast. As a test of validity of the computational method, we first determine the potential energy as a function of atomic volume; the potential energy of an individual atom in vacuum is zero. From this function, we further derive equilibrium lattice constants, bulk moduli, and their derivatives with respect to pressure of the α, β and γ phases. Shown in Fig. 2 is the potential energy E_U as a function of atomic volume. Consistent with experimental observation[1], the α phase is more stable than γ phase at 0K; or the binding of α phase is stronger than γ phase. For the α phase, our calculation results with scalar (PAW+scalar) and with spin-orbital (PAW+SO) interactions are compared with available experimental results[2,3] and full potential linear muffin-tin orbital theory with spin-orbital (FPLMTO+SO) interactions results[13] in Table I; the experimental measurements of lattice constants are at 4K, and the modulus at room temperature. In terms of lattice constants and bulk modulus, our results with scalar or spin-orbital interactions are close to both experimental values and previous calculation results. The experimental value of B' (pressure derivative of bulk modulus B) is smaller than our result and previous calculation result, and this discrepancy could be the result of finite temperature and Birch-Murnagan fitting over large volume range. When it comes to γ phase without spin-orbital interaction, our calculations show that the bulk modulus is 122.6 GPa and its pressure derivative is 4.1; these compare well with the experimental values of 113.3 GPa and 3.4 [2]. All these results show that the PAW and GGA together can reproduce the experimental results for pure U, with or without spin-orbital interactions. This feasibility test is consistent with another report on defects in uranium nitride using the same method.[23]

Table I. The properties of α phase. Atomic volume V_0 in unit of Å^3, lattice constants (a, b, c, and y) in unit of Å, bulk modulus B in unit of GPa and its pressure derivative B'.

	V_0	a	b	c	y	B	B'
PAW+SO	20.7484	2.8318	5.9403	4.9337	0.09713	142.3	5.0
PAW+scalar	20.1012	2.8014	5.8821	4.8795	0.09719	142.5	5.0
FPLMTO+SO	20.67	2.845	5.818	4.996	0.1025	133.0	5.4
Experiments	20.5815	2.8444	5.8689	4.9316	0.10242	135.5	3.8

In addition to the energies, electron distributions are vital to bonding and thereby defect formation in U. As Fig. 3 shows, the 6s and 6p electrons in the α phase are relatively deep into the core and not valence electrons; this is also true for β and γ phases. Their inclusion may be redundant for most calculations, and is an extra safety of reliability. In other words, Fig. 3 indicates that our calculations have included more than sufficient valence electrons. Among all electrons, the f-electrons dominate near the Fermi surface E_F. The dominance of f-electrons applies to all the three phases (α, β, and γ), as shown in Fig. 4.

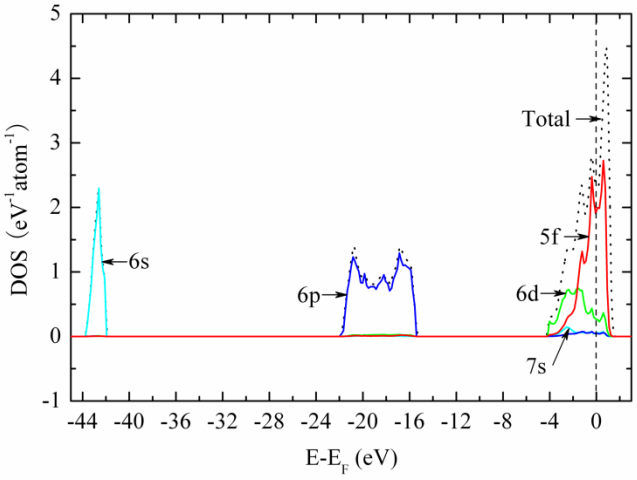

Fig. 3. (color online) Partial and total densities of state (DOS) in equilibrium α phase, with 5f, 6s, 6p, 6d, and 7s electrons labeled. The energy E is relative to the Fermi surface E_F.

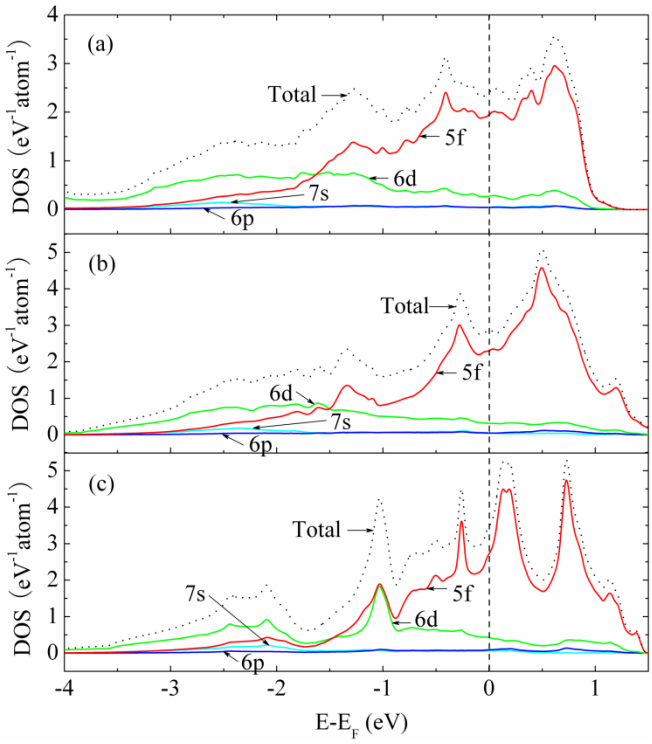

Fig. 4. (color online) Partial and total densities of state (DOS) in equilibrium (a) α, (b) β, and (c) γ phases, near the Fermi surface. The energy E is relative to the Fermi surface E_F.

From the distribution of electrons in energy space, we now turn to the distribution in real space. For clear visualization, we use two-dimensional density contours on high-symmetry and high atom-density planes, to illustrate the electron density between first-nearest, second-nearest and third-nearest neighbors. For consistency, solid contour lines for all three phases represent electron densities from 0.38 Å^{-3} to 0.33 Å^{-3}, 0.28 Å^{-3}, and 0.23 Å^{-3}. Nowhere in a perfect crystal is the electron density below 0.18 Å^{-3}. The dotted contours correspond to electron density of 1.00 Å^{-3} and outline core regions of atoms.

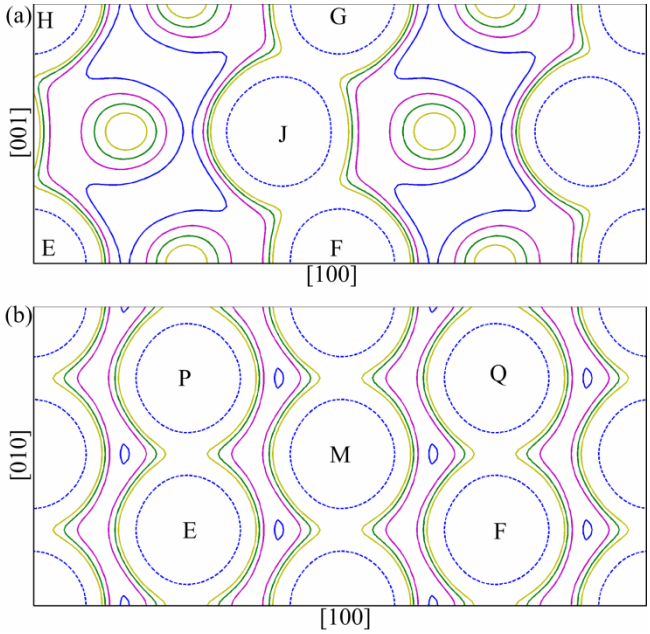

Fig. 5. (color online) Electron density contours of α phase.

We first examine the electron distribution in each phase, and then compare the distributions among the three phases. As shown in Fig. 5 (a), the electron density between two first nearest neighbors F and J (notations as defined in Fig. 1) in the α phase is always higher than 0.38 Å^{-3}. The region of such high electron density between two second nearest neighbors F and Q is relatively narrower; Fig. 5(b). When it comes to two third nearest neighbors F and M, the electron density can be lower than 0.28 Å^{-3} (although still higher than 0.23 Å^{-3}); Fig. 5(b).

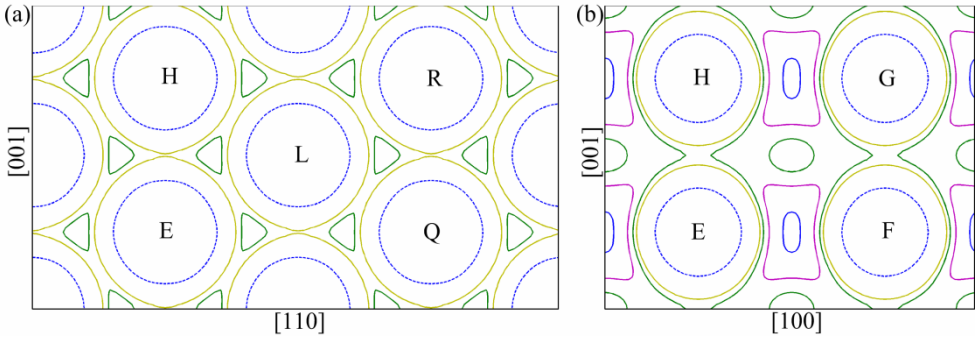

Fig. 6. (color online) Electron density contours of β phase.

The electron density variation in the β phase is similar to that in the α phase. As shown in Fig. 6 (a) for β phases U, the electron density between two first nearest neighbors E and H in the β phase can reach 0.38 Å^{-3} over very short distance. The electron density between two second nearest neighbors E and L cannot reach 0.38 Å^{-3} (although still higher than 0.33 Å^{-3}; Fig. 6 (a). When it comes to two third-nearest neighbors E and F, the electron density can be lower than 0.23 Å^{-3}; Fig. 6 (b).

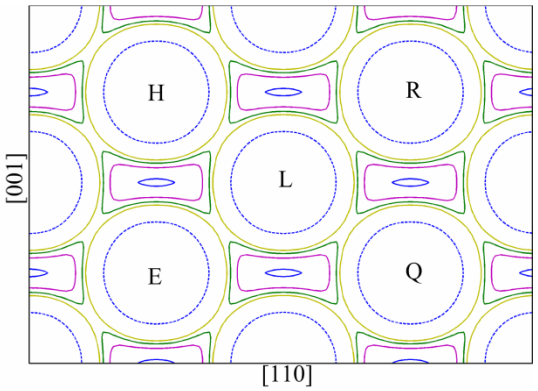

Fig. 7. (color online) Electron density contours of γ phase.

The electron density variation in the γ phase (Fig. 7) follows the same trend as in the two other phases. The electron density between two first nearest neighbors E and L can lower than 0.38 Å^{-3} (but still higher than 0.33 Å^{-3}). Between two second nearest neighbors E and H, or two third nearest neighbors E and Q, the electron density can be lower than 0.23 Å^{-3}; the difference is that the distance of such low density is smaller between second than between third nearest neighbors.

Comparing electron density distributions in the three phases, we note that the density is the most inhomogeneous in the α phase, and the least in the γ phase; the β phase is in between. In the α phase, the lowest density between two first nearest neighbors is higher than 0.38 Å^{-3}; while the lowest is approaching 0.18 Å^{-3} for all phases. In contrast, the

lowest density between two first nearest neighbors in the γ phase is lower than 0.38 $Å^{-3}$.

The variation of electron density homogeneity correlates with the symmetry of crystal structures. The inhomogeneous distribution in a phase correlates with low symmetry, and the relatively more homogeneous distribution in γ phase correlates with cubic symmetry.

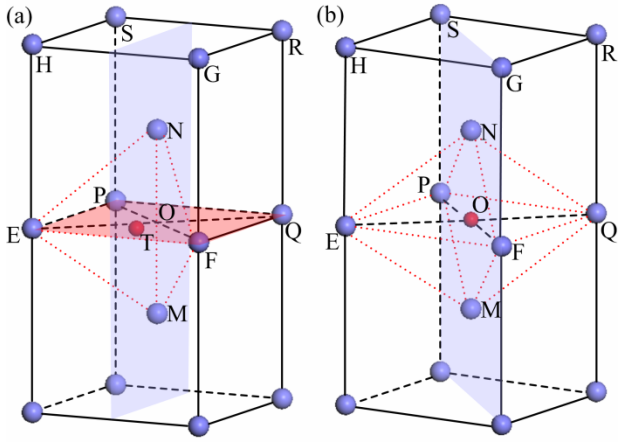

Fig.8. (color online) Atomic configurations of (a) a tetrahedral (T) and (b) an octahedral (O) interstitial site in γ phase.

The electron distribution also affects defect formation energies. The formation energy of a single vacancy is 1.08 eV, that of a Nb substitution 0.59 eV, that of Nb interstitial at a tetrahedral site 1.58 eV, and that of Nb interstitial at an octahedral site 2.35 eV. The atomic configurations of a single vacancy and an Nb substitution need no further elaboration. The octahedral (O) and the tetrahedral (T) sites are shown in Fig. 8; labels of lattice sites follow the same notations of Fig. 1. The octahedral site is at the center of a {001} face PEFQ and also the bottom of {110} face FGSP. The tetrahedral site is also on the {001} face PEFQ; however, it is at the middle of point O and line EF and is also equal distant to points E and F.

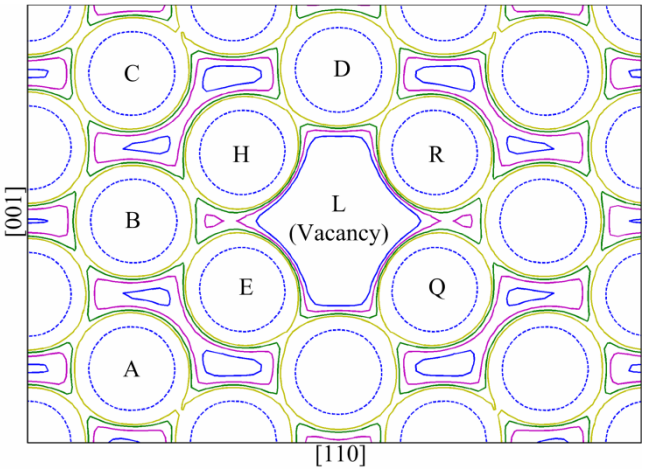

Fig. 9. (color online) Electron density contours around a vacancy in γ phase.

Near each defect, electron distribution varies from its perfect crystal counterpart. As shown in Fig. 8, the most prominent changes occur around the first nearest neighbors E, H, Q, and R of the vacancy L. The nearest neighbors relax toward the vacancy. As a result, the electron density between such a neighbor and its own neighbor (such as H and C) substantially decreases; from above 0.38 $Å^{-3}$ to below 0.33 $Å^{-3}$. This decrease of local electron density may help facilitate vacancy diffusion by enabling the first nearest neighbors (such as H) to jump to the vacancy site L.

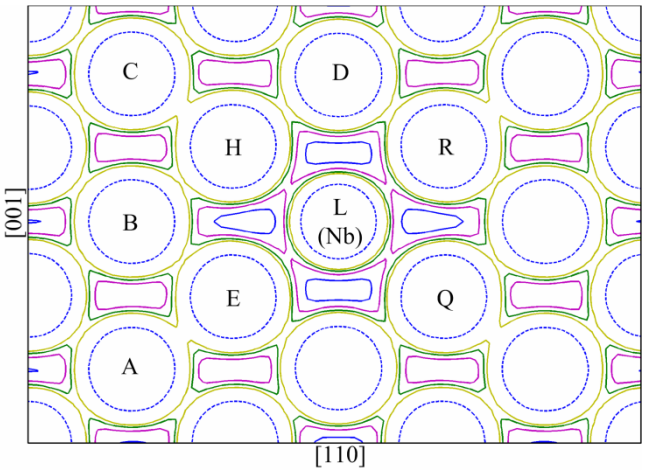

Fig. 10. (color online) Electron density contours around a substitutional Nb in γ phase.

Once the vacancy site is occupied by an Nb atom, the configuration corresponds to a Nb substitution. As shown in Fig. 10, the Nb substitution does not perturb the electro

density between H and C as much as the vacancy does. However, the Nb substitution does substantially reduce the electron density between H and E (who are second nearest neighbors) and between H and R (who are third nearest neighbors). The electron density varies sharply around the Nb atom, and the sharpness is probably responsible for the small perturbation of electron density between two nearest neighbors H and C. The small perturbation in turn explains the small formation energy of substitutional Nb.

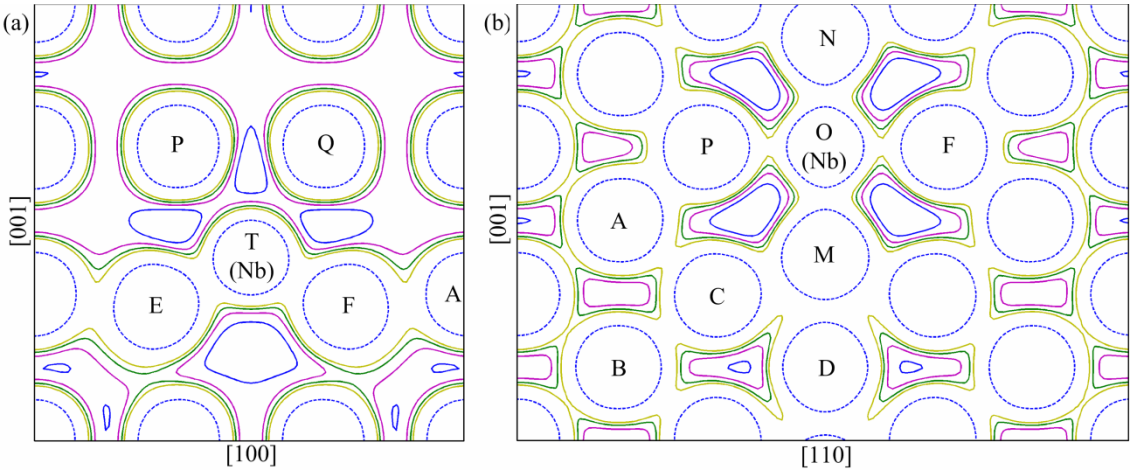

Fig. 11. (color online) Electron density contours around a Nb interstitial at (a) a tetrahedral site and (b) an octahedral site in γ phase.

The change of electron density distribution near an Nb interstitial is much more prominent. As shown in Fig. 11 (a), around the tetrahedral site four large regions of low electron density appear, and the electron density between F and A (who are the second nearest neighbors) increases substantially. Around an octahedral site, as shown in Fig. 11 (b), the change is even more prominent; the four regions of low density are wider, and the density between for example M and C goes up even more. The prominent changes correlate well with the large formation energies of Nb interstitials.

Before closing, we also note that two substitutional Nb atoms do not prefer clustering. When two substitutional Nb atoms are nearest neighbors, the formation energy is 1.32 eV; which is 0.14 eV higher than the sum of formation energies of two separate substitutional Nb atoms.

IV. CONCLUSIONS

In summary, we have used density-functional-theory based *ab initio* calculations to investigate Nb in U. Our calculations show: (1) f-electrons dominate the population near Fermi surface of pure U (true for all three phases); (2) formation energies of single vacancy, Nb substitution, Nb interstitial at tetrahedral site, and Nb interstitial at octahedral site in γ phase of U are 1.08 eV, 0.59 eV, 1.58 eV, and 2.35 eV, respectively;

(3) electron density distribution changes less near a substitutional Nb than near an interstitial Nb, and such changes correlates with variations of formation energies. Based on the formation energies, the thermodynamically preferable site of Nb in γ phase U is the substitutional site. Further, two substitutional Nb atoms have higher formation energy as nearest neighbors than as separate entities.

ACKNOWLEDGMENTS

The work is carried out through primary support of UC, Lawrence Livermore National Laboratory under the auspices of the US Department of Energy under Contract No. W-7405-Eng-48. The authors SX and HH also acknowledge support of National Science Foundation through the following programs: Partnerships for Advanced Computational Structure, Distributed Terascale Facility (DTF) and Terascale Extensions: Enhancements to the Extensible Terascale Facility.

Reference

1 E. Yu Tonkov and E. G. Ponyatovsky, *Phase Transformations of Elements under High Pressure* (CRC Press, Boca Raton, 2005).

2 C. S. Yoo, H. Cynn, and P. Söderlind, Phys. Rev. B **57**, 10359 (1998).

3 C. S. Barrett, M. H. Mueller, and R. L. Hitterman, Phys. Rev. **129**, 625 (1963).

4 H. G. Smith, N. Wakabayashi, W. P. Crummett, R. M. Nicklow, G. H. Lander, and E. S. Fisher, Phys. Rev. Lett. **44**, 1612 (1980).

5 B. Mihaila, C. P. Opeil, F. R. Drymiotis, J. L. Smith, J. C. Cooley, M. E. Manley, A. Migliori, C. Mielke, T. Lookman, A. Saxena, et al., Phys. Rev. Lett. **96**, 076401 (2006).

[6] E. S. Fisher and D. Dever, Phys. Rev. **170**, 607 (1968).

[7] J. Zhou and L. M. Hsiung, J. Mater. Res. **21**, 013523 (2006).

[8] D W. Brown, R E. Hackenberg, D F. Teter, M A. Bourke and D Thomas, Los Alamos Science, **30**, 78 (2006).

[9] P. Söderlind, Adv. Phys. **47**, 959 (1998).

[10] M. D. Jones, J. C. Boettger, R. C. Albers, and D. J. Singh, Phys. Rev. B **61**, 4644 (2000).

[11] P. Söderlind, Phys. Rev. B **66**, 085113 (2002).

[12] L. Fast, O. Eriksson, B. Johansson, J. M. Wills, G. Straub, H. Roeder, and L. Nordström, Phys. Rev. Lett. **81**, 2978 (1998).

[13] J. P. Crocombette, F. Jollet, L. T. Nga, and T. Petit, Phys. Rev. B **64**, 104107 (2001).

[14] M. Freyss, T. Petit, and J. P. Crocombette, J. Nucl. Mater. **347**, 47 (2005).

[15] G. Kresse and J. Furthm ller, Phys. Rev. B **54**, 11169 (1996).

[16] G. Kresse and D. Joubert, Phys. Rev. B **59**, 1758 (1999).

[17] J. P. Perdew and Y. Wang, Phys. Rev. B **45**, 13244 (1992).

[18] L. G. Zhou and H. Huang, Appl. Phys. Lett. 84, 1940 (2003).

[19] F. Birch, Phys. Rev. **71**, 809 (1947).

[20] M. D. Segall, R. Shah, C. J. Pickard, and M. C. Payne, Phys. Rev. B **54**, 16317 (1996).

[21] E. A. Kotomin, R. W. Grimes, Y. Mastrikov, and N. J. Ashley, J. Phys.: Condens. Matter **19**, 106208 (2007)